Reduced Temperature Dependence of Collective Conformational Opening in a Hyperthermophile Rubredoxin

Griselda Hernández* and David M. LeMaster

Wadsworth Center and Department of Biomedical Sciences, University at Albany-State University of New York, Empire State Plaza, Albany, New York 12201-0509

Received June 18, 2001; Revised Manuscript Received August 28, 2001

ABSTRACT: Spatially localized differences in the conformational dynamics of the rubredoxins from the hyperthermophile *Pyrococcus furiosus* (*Pf*) and the mesophile *Clostridium pasteurianum* (*Cp*) are monitored via amide exchange measurements. As shown previously for the hyperthermophile protein, nearly all backbone amides of the *Cp* rubredoxin exhibit EX_2 hydrogen exchange kinetics with conformational opening rates of $>1\ s^{-1}$. Significantly slower amide exchange is observed for *Pf* rubredoxin in the region surrounding the metal site and the proximal end of the three-stranded β-sheet, while for the rest of the structure, the exchange rates at 23 °C are similar for both proteins. For the multiple-turn region comprising residues 14−32 in both rubredoxins, the uniformity of both the exchange rate constants and the values of the activation energy at the slowly exchanging sites is consistent with a model of solvent exposure via a subglobal cooperative conformational opening. In contrast to the common expectation of increased rigidity in the hyperthermophile proteins, below room temperature *Pf* rubredoxin exhibits a larger apparent flexibility in this multiple-turn region. The smaller enthalpy for the conformational opening process of this region in *Pf* rubredoxin reflects the much weaker temperature dependence of the underlying conformational equilibrium in the hyperthermophile protein.

The characterization of hyperthermophilic organisms that grow optimally at >80 °C has stimulated numerous structural comparisons between individual hyperthermophile proteins and their homologues from more temperate organisms (*1*−*3*). Although certain structural correlations, such as an increased number of salt bridges in the thermophile proteins (*4*−*6*), have been observed, enhanced thermal stability appears to involve the accumulation of numerous subtle structural interactions. Indeed, it is open to question whether focusing strictly on native state interactions is sufficient for adequately predicting differences in global thermodynamic equilibria. Recently, more attention has turned to the question of a possible dynamical basis for thermal stability following the paradigm that enhanced conformational rigidity in the native state may account for increased thermostabilization (*7*, *8*). Nearly all experimental comparisons of thermophile and mesophile proteins reported to date suggest an increased rigidity of the thermostable homologue. These studies have drawn primarily on FT-IR monitoring of the aggregate amide exchange kinetics (*9*−*12*) as well as tryptophan fluorescence (*13*) and phosphorescence (*14*) lifetimes and fluorescence depolarization measurements (*15*). However, inelastic neutron scattering studies have indicated an opposite conclusion of increased heavy atom fluctuations in a more thermostable α-amylase (*16*).

Each of these studies is limited by the constraint that only a structurally averaged (FT-IR amide exchange and neutron scattering) or highly localized (fluorescence and phosphorescence) conformational behavior is monitored. In contrast, NMR provides monitoring of individual sites throughout the structure. Furthermore, evidence of collective modes of motion can be obtained when a spatially localized set of amides exhibit similar but characteristic exchange behavior as a function of protein destabilization, such as by variation of temperature or guanidinium concentration (*17*). Recently, Hollien and Marqusee (*18*) reported the conventional deuterium exchange kinetics for approximately one-third of the amides of the thermophile *Thermus thermophilus* RNase H and compared these data to the data from their earlier study of the *Escherichia coli* enzyme (*19*). They reported that the amide protection factors were proportionally increased at nearly all residue positions for the *T. thermophilus* protein, indicating a delocalized mechanism of thermal stabilization.

With regard to the spatial distribution of thermal stabilization, a molecular dynamics comparison between a wild-type subtilisin and a thermostable homologue generated by directed evolution concluded that, although several specific regions had reduced fluctuations, the thermostabilized subtilisin has on average a higher flexibility (*20*). Although an analogous molecular dynamics comparison of the rubredoxin from the hyperthermophilic *Pyrococcus furiosus* (*Pf*)[1] and a mesophile homologue predicted an increased number of fluctuations in the mesophile rubredoxin at room temperature (*21*), Karplus and co-workers emphasized that there is no necessary correlation between conformational rigidity and

* To whom correspondence should be addressed.

[1] Abbreviations: *Cp*, *Clostridium pasteurianum*; *Pf*, *Pyrococcus furiosus*; CLEANEX-PM, CLEAN chemical exchange spectroscopy, phase-modulated; FHSQC, fast heteronuclear single-quantum correlation; k_{ex}, observed amide exchange rate; k_{op}, rate of conformational opening to an exchange competent state; k_{cl}, rate of conformational closing to a nonexchanging state; k_{ch}, rate of hydrogen exchange from the exchange competent state; k_{OH^-}, $k_{ex}/[OH^-]$.

10.1021/bi0112560 CCC: $20.00 © 2001 American Chemical Society
Published on Web 11/07/2001

global thermodynamic stability. Furthermore, they pointed out that flexibility comparisons require a time frame reference. In particular, fluorescence and phosphorescence, inelastic neutron scattering, and molecular simulations are sensitive to motion in the picosecond to nanosecond time frame, while under most circumstances, conventional amide exchange experiments provide only the kinetic constraint of an upper limit to conformational opening events on the scale of hours to months.

The conformational kinetics information of an amide exchange experiment can be markedly enhanced by directly observing the transfer process of ^{1}H spins from the bulk solvent resonance to the individual amide resonances. By this means exchange rates of greater than $\sim$0.5 s^{-1} and less than $\sim$100 s^{-1} can be monitored. Given suitable protein stability, increases in pH and temperature allow for at least a 10^8-fold range of rate constants to pass within the time window of the magnetization transfer experiment. Hence, the exchange kinetics for essentially all amide sites of a protein can be determined. Previously, we (*22*) demonstrated that throughout the structure of *Pf* rubredoxin, the most thermostable protein characterized to date (*23*), the amides can open for exchange in less than 1 s near room temperature. Herein, we present a comparison of the exchange behavior of *Pf* rubredoxin with that from the mesophilic *Clostridium pasteuranium* (*Cp*). Differences in the exchange rates and in the activation energies of exchange are interpreted in terms of the structural distribution and collective modes of exchange.

EXPERIMENTAL PROCEDURES

Preparation of Isotopically Labeled Rubredoxins. Synthetic codon usage-optimized genes for both *C. pasteuranium* (*24*, *25*) and *P. furiosus* rubredoxin (*25*), cloned into the pT7-7 vector, were used for protein expression (both plasmids kindly provided by M. K. Eidsness, University of Georgia, Athens, GA). The *Cp* rubredoxin plasmid was transformed into BL21(DE3) and grown in M9 glucose minimal medium in which 1 g/L $^{15}NH_4Cl$ was substituted. Expression of *Pf* rubredoxin followed a similar protocol in which the M9 glucose minimal medium was prepared in ^2H_2O and additionally supplemented with the RPMI 1640 vitamins mixture (Sigma-Aldrich). Purification of the *Cp* rubredoxin generally followed published procedures (*24*, *26*). Ammonium sulfate fractionation (pellet saturated 40−90%) was followed by gel filtration on Sephadex G-50 in 50 mM Tris-HCl (pH 7.5) with a subsequent step of ion exchange chromatography on QAE-Sephadex G-25 in the same buffer with a NaCl gradient to 0.6 M. The early stages of the purification of *Pf* rubredoxin followed an identical procedure with the eluant from the QAE-Sephadex column being dialyzed into 50 mM Tris-HCl (pH 8.5) and then chromatographed on hydroxyapatite to remove the residual *N*-formylmethionine and fully processed forms (*25*). Mass spectral analysis of the ^{2}H- and ^{15}N-labeled N-terminal methionine form *Pf* rubredoxin indicated an average deuteration level of >95%.

NMR Spectroscopy. Samples of 3 mM ^{15}N-labeled *Cp* rubredoxin and 3 mM ^{2}H- and ^{15}N-labeled *Pf* rubredoxin were both dialyzed against two 30 mL aliquots of the same 7% ^2H_2O buffer solutions composed of 0.1 M sodium chloride, 0.02 M sodium phosphate, and 0.02 M boric acid titrated to the required pH with sodium hydroxide. [Note that both boric acid and the third ionization of phosphate have heats of ionization of $\sim$3.5 kcal/mol (*27*, *28*).] All NMR data were collected on a Bruker DRX 500 spectrometer and processed in FELIX (Molecular Simulations) using cosine bell weighting functions. The previously published amide resonance assignments for *Cp* rubredoxin (*29*) were amended by the interchange of the assignments for Asp 21 and Asp 29, as well as for Asn 25 and Asp 35, based on NOESY, TOCSY, and long-range heteronuclear coupling analysis.

Clean chemical exchange-phase modulated (CLEANEX-PM) (*30*) and FHSQC (*31*) spectra were collected as a function of pH and temperature. At 42 and 51 °C, a relaxation delay of 4 s was used, while a value of 2 s was used at lower temperatures. Following the highest-temperature experiment at each pH value, the data sets for the next lower temperature were recollected to test them against artifacts of sample degradation. ^1H_2O T_1 relaxation corrections were carried out as previously described (*30*). As reported previously for *Pf* rubredoxin (*22*), the effects of incomplete cancellation between rotating-frame and longitudinal nuclear Overhauser effects were negligible. For ^{15}N-labeled *Cp* rubredoxin, CLEANEX-PM mixing times of 5.19, 10.38, 15.57, and 20.76 ms were used. Taking advantage of the more favorable relaxation rates in the ^{2}H- and ^{15}N-labeled sample, we used mixing times of 7.14, 14.28, 21.42, 28.56, and 35.70 ms for *Pf* rubredoxin. Independent of the initial rate values, a modest downward deviation was observed for the CLEANEX-PM buildup curves. The median deviation for the ^{15}N-labeled *Cp* rubredoxin data corresponded to a nominal T_2 value of 75 ms, while for the ^{2}H- and ^{15}N-labeled *Pf* rubredoxin, the median value increased to 225 ms. These median corrections were applied to each CLEANEX-PM mixing time data set in deriving the estimated rate of recovery toward the reference FHSQC peak intensities. Deviations in the fit values consistent with the *Cp* rubredoxin experimental noise levels were obtained for exchange rates in the range of 0.5−50 s^{-1}. The increased peak intensities, combined with the longer practical mixing times of the perdeuterated samples, allowed accurate exchange rates for the ^{2}H- and ^{15}N-labeled *Pf* rubredoxin to be obtained down to 0.2 s^{-1}.

RESULTS AND DISCUSSION

Pf and Cp Rubredoxin Amide Exchange Kinetics at 23 °C. Conformationally protected amide hydrogens exchange with solvent according to the general scheme

$$\text{closed} \underset{k_{cl}}{\overset{k_{op}}{\rightleftarrows}} \text{open} \xrightarrow{k_{ch}} \text{exchanged}$$

The observed exchange kinetics (k_{ex}) depend on these rate constants according to (*32*)

$$k_{ex} = k_{op}k_{ch}/(k_{op} + k_{cl} + k_{ch})$$

Exchange can only occur following a conformational opening transition. When that opening transition is rate-limiting, k_{op} equals k_{ex} and the so-called EX_1 condition is met. In most protein studies, the rate of conformational closing (k_{cl}) has been found to be much greater than the chemical exchange

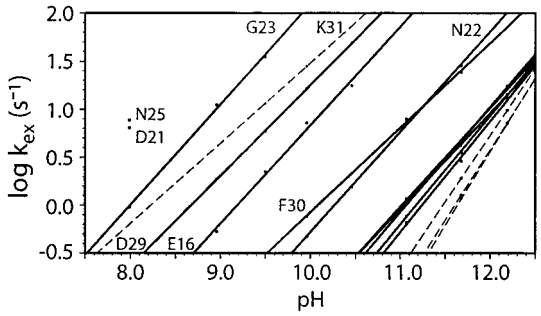

FIGURE 1: Amide exchange rates for all non-prolines in residues 14−32 of *Cp* rubredoxin as a function of pH at 23 °C. For each residue, a least-squares fit to the experimental data is illustrated. Dashed lines are drawn for residues having data from only two pH values. Data for the more weakly protected amides are identified by residue name.

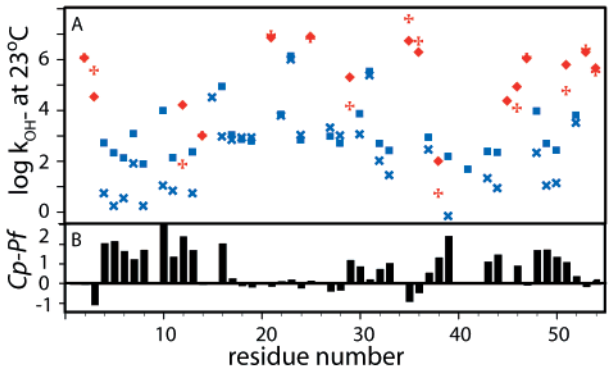

FIGURE 2: Amide exchange rate constants for *Cp* and *Pf* rubredoxins at 23 °C. The log k_{OH^-} value for poly(D,L-alanine) is 8.3 under these conditions (*43*, *52*). In panel A, red symbols denote residues that are exposed to solvent in the X-ray structure while blue symbols denote the solvent inaccessible sites. As shown in panel B, for nearly all amides the rate constants for *Pf* rubredoxin (+ and ×) are equal to or smaller than those for *Cp* rubredoxin (◆ and ■) at this temperature. Exchange rate constants are derived from the pH range in which the magnetization transfer kinetics are observed (generally, 1 s^{-1} < k_{ex} < 30 s^{-1}).

rate of the exposed amide (k_{ch}), the so-called EX_2 condition. In this case, k_{op} is necessarily larger than k_{ex}. In the conventional ^2H_2O exchange out experiment, the observed amide exchange rate k_{ex} is commonly in the range of hours to months which provides a rather weak kinetic constraint to the underlying conformational opening rate. However, the magnetization transfer-based experiment utilized herein monitors amide exchange rates up to nearly 100 s^{-1}, at least 10^4 −10^5 times faster than the rates commonly detected in ^2H_2O exchange out experiments. Hence, the kinetics of the underlying conformational opening process can be much more strongly constrained.

The CLEANEX-PM (*30*, *33*) experiment measures the fraction of the amide sites which become conformationally available for exchange during a variable pulse mixing period. If exchange of ^1H magnetization between the amide site and the bulk water resonance becomes too rapid (approximately >100 s^{-1}), the amide resonance becomes broadened beyond detection. More significant in the present context is the fact that conformational opening processes that are substantially slower than ∼0.2 s^{-1} can only give rise to a signal that is proportionate to k_{op}/k_{cl} which in most cases is far too small to observe. The unfolding rate of *Cp* rubredoxin is ∼1 h^{-1} at 80 °C and pH 7, while *Pf* rubredoxin unfolds 10^2−10^3 times more slowly (*34*). As a result, the global unfolding process does not contribute to the amide exchange kinetics described in these experiments.

Under the alkaline conditions used in this study, if the effects of other ionization events can be ignored, EX_2 kinetics imply that the observed exchange rate k_{ex} will be proportional to [OH^-]. For the Zn^{2+} form of both *Pf* and *Cp* rubredoxin, CLEANEX-PM and reference FHSQC (*31*) spectra were collected at 4.5, 14, 23, 32.5, 42, and 51 °C at pH 7.99, 8.96, 9.96, 11.07, and 12.19 (at pH 12.19 only up to 42 °C for *Cp* rubredoxin). In addition, spectra were collected on *Cp* rubredoxin at 23 °C at pH 9.50, 10.46, and 11.68 to facilitate verification of EX_2 kinetics. Consistent with the previously reported results for the hyperthermophile protein (*22*), EX_2 behavior was verified for nearly all residues of the mesophile *Cp* rubredoxin. As illustrated in Figure 1, all of the non-proline residues in the segment of amino acids 14−32 exhibit a log−log slope near 1.0, indicating EX_2 kinetics for exchange rates up to at least 30 s^{-1}. For the residues in which exchange rates were obtained at either three or four different pH values, the apparent slope of the log k_{ex} versus pH best fit lines varied from 0.88 to 1.15.

In Figure 2A are plotted the log k_{OH^-} (=k_{ex}/[OH^-]) values at 23 °C for the amides of both rubredoxins. The upper bound of the graph approximates the intrinsic rate of a fully exposed peptide. The red symbols denote amides which are accessible to solvent (*35*) in the high-resolution X-ray structures (*36*, *37*) (ACCESS program kindly provided by F. M. Richards, Yale University, New Haven, CT). At nearly every position of the mesophile *Cp* rubredoxin (◆ and ■), the exchange rate is equal to or higher than that of the hyperthermophile protein (+ and ×). Indeed, the mesophile protein exchanges at a substantially slower rate for only three weakly protected, solvent-exposed amide positions. On the other hand, the distribution of differential exchange rates along the protein sequence is highly nonuniform (Figure 2B). The structural localization of the differential exchange rates is more readily apparent when the residues showing at least 10-fold faster exchange in the mesophile *Cp* rubredoxin are colored red in its X-ray structure (Figure 3A). The differential amide protection is localized to the region surrounding the metal binding site and the proximal end of the three-stranded β-sheet. The obvious exceptions in the lower portion of the figure are Glu 16 and Asp 29 which are immediately adjacent to the much discussed interaction between residues 15 and 30.

In the initial X-ray structural analysis of *Pf* rubredoxin (*38*), Rees and co-workers discussed potential structural correlates for its extreme thermal stability. In particular, they noted the presence of a tertiary ionic hydrogen bond between the side chain carboxyl of Glu 15 (*Cp* rubredoxin numbering) and the main chain amide of Phe 30 and the side chain indole of Trp 4. In general, mesophile rubredoxins lack both Glu at position 15 and Trp at position 4. In addition, under more neutral pH conditions, the wild-type *Pf* rubredoxin also has a salt bridge between the other oxygen of the Glu 15 carboxyl and the N-terminal ammonium group. In the *E. coli*-expressed sample studied here, the N-terminal methionine is not efficiently processed (*25*), thus adding an additional residue and converting the salt bridge of the native form to an ionic hydrogen bond with the amide of Ala 2 (*37*).

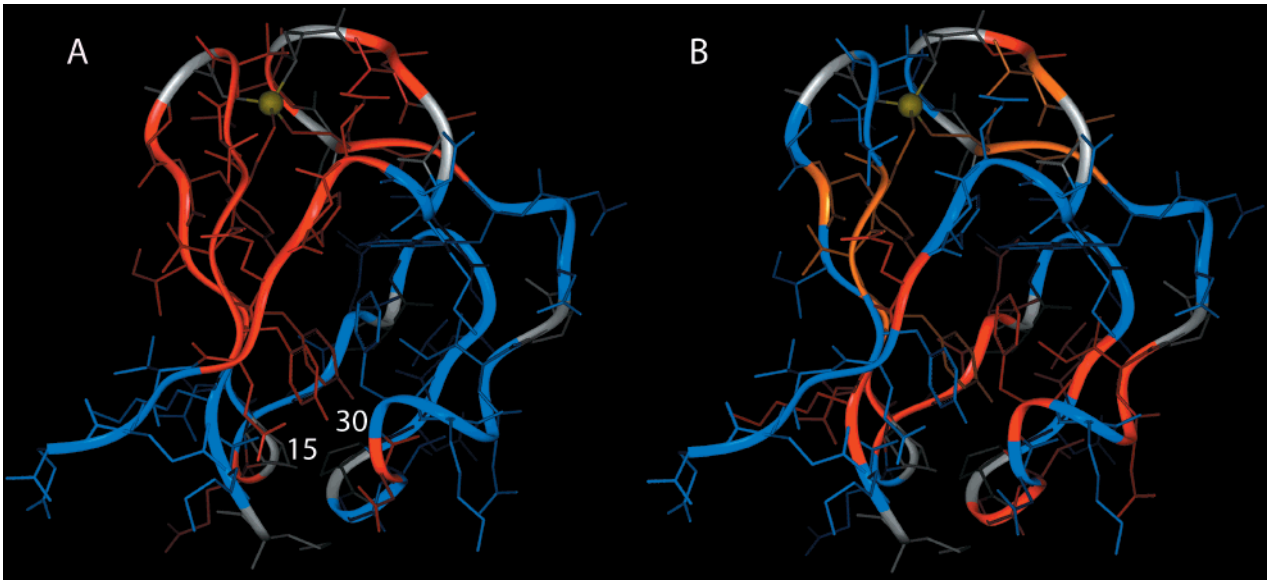

FIGURE 3: Spatial distribution of differential exchange rates for *Cp* vs *Pf* rubredoxin and elevated activation energies of exchange in *Cp* rubredoxin. In panel A, amides that exchange at least 10-fold more rapidly in *Cp* rubredoxin are marked in red. Positions with smaller differential exchange rate constants are marked in blue, while amide positions lacking experimental data, including the five prolines, are shown in gray. Amides exhibiting large differential exchange rates are primarily located around the Zn^{2+} (yellow) binding site and the proximal end of the three-stranded β-sheet. The two exceptions located in the lower portion of the figure, Glu 16 and Asp 29, are immediately adjacent to the site of the buried ionic hydrogen bond between Glu 15 and Phe 30 that occurs only in the hyperthermophile rubredoxin structure. The *Cp* rubredoxin structure (*36*) given here indicates the Pro 15 substitution. In panel B, residues of *Cp* rubredoxin exhibiting an activation energy of amide exchange at least 4 kcal/mol higher than that observed in *Pf* rubredoxin are colored red. Residues for which *Pf* rubredoxin has k_{OH^-} values of <30 s^{-1} and for which *Cp* rubredoxin has activation energies >4 kcal/mol above the free peptide value are colored in orange. Blue denotes residues having smaller differential activation energies, while residues lacking experimental data are denoted in gray.

Stability studies indicate that the wild-type protein is only modestly more stable than the Met terminal form (*25*, *37*).

Although the metal cluster may account for the significant thermal stability of both rubredoxins [*Cp* rubredoxin denatures near 80 °C (*26*), and *Pf* rubredoxin appears to denature in the range of 170−200 °C (*23*)], it cannot explain the differential stability of these two proteins. Since the *Pf* protein remains more stable than *Cp* rubredoxin down to pH 2 where the salt bridges are disrupted, enhanced hydrophobic stabilization of *Pf* rubredoxin has been proposed (*34*). To test whether metal binding might be responsible for the irreversibility of thermal denaturation of *Pf* rubredoxin, substitutions for the four coordinating cysteines yielded a rubredoxin variant, lacking the metal cluster, which forms a nativelike conformation that reversibly denatures at 82 °C and pH 7 (*39*). When the analogous mutations were introduced into a mesophile rubredoxin, folding to a nativelike structure could not be achieved. Similar stability differences have been observed in the comparison of the metal-free forms of wild-type *Pf* and *Cp* rubredoxins (*40*).

With regard to the interactions in the proximal end of the β-sheet, the hydrophobic interactions among Val 5, Ile 12, and Leu 52 of the three strands have been proposed to contribute to the increased stability of *Pf* rubredoxin (*41*), although disruption of this interaction appears to have a minimal effect on stability (*25*). Similarly, only the hyperthermophile protein has a salt bridge between Lys 7 and Glu 50 linking the first and third β-strands (*38*), but in this case again, mutagenesis studies indicate at most a modest role in stabilization (*42*).

Conformational Enthalpies of Rubredoxin Amide Exchange. A different perspective emerges when the temperature dependence of the amide exchange is considered. As noted previously (*22*), the activation energies of exchange for the large majority of the residues in the hyperthermophile *Pf* rubredoxin are within 3−4 kcal/mol of the free peptide value of 17 kcal/mol (*43*). Residues exhibiting k_{OH^-} values of <30 s^{-1} at 23 °C exchanged too slowly for reliable determination of the temperature dependence. In marked contrast, nearly half of the amides of *Cp* rubredoxin exhibit activation energies of exchange more than 4 kcal/mol above the free peptide value. Figure 4 illustrates the Arrhenius plot for the amide exchange rates of residues 16 and 30 of both rubredoxins. In both proteins, residue 16 exhibits an activation energy typical of a free peptide. Although Phe 30 of the hyperthermophile protein exhibits a similar temperature dependence, this residue in *Cp* rubredoxin exhibits a substantially higher activation energy of exchange. Under the observed EX_2 kinetics conditions, the exchange rate reflects a conformational pre-equilibration between the open and closed states with a subsequent chemical exchange step. If it is assumed only that the activation energy of the chemical exchange step is the same for Phe 30 in either protein, the observed differential temperature dependence directly determines the differential enthalpy of the conformational equilibrium according to

$$\mathrm{d}(\ln K)/\mathrm{d}(1/T) = -\Delta H/R$$

Within the precision of these exchange data, there is a linear differential temperature dependence between the Phe 30 residues of *Pf* and *Cp* rubredoxins, indicating that the differential enthalpy of the relevant conformational opening is essentially constant over the observed temperature range.

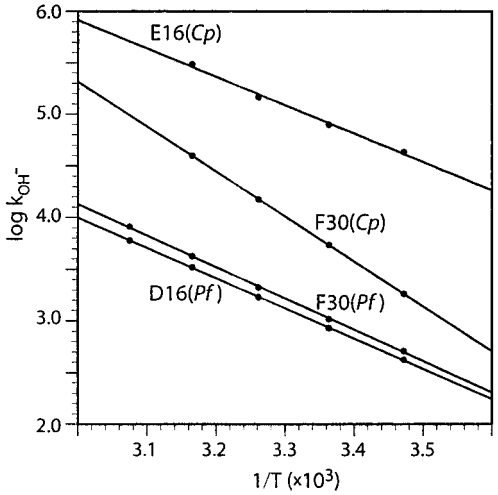

FIGURE 4: Arrhenius plot for the amide exchange kinetics of residues 16 and 30 from *Cp* and *Pf* rubredoxins. Phe 30 of *Cp* rubredoxin shows a significantly steeper temperature dependence than does either Phe 30 of *Pf* rubredoxin or residue 16 from either protein. The latter three amides exhibit activation energies similar to that of a free peptide [i.e., 17 kcal/mol (*43*)].

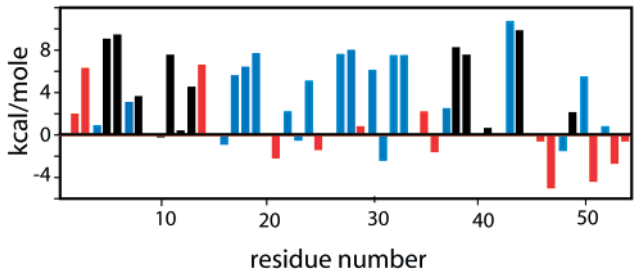

FIGURE 5: Elevated activation energies of amide exchange in *Cp* rubredoxin. In cases for which activation energies are available for both *Cp* and *Pf* rubredoxin, subtraction yields the differential enthalpy for the conformational opening process. For such residues, red denotes residues that are solvent-exposed in the crystal structure, while solvent inaccessible sites are colored blue. For *Pf* rubredoxin residues in which accurate activation energies of exchange could not be obtained (i.e., k_{OH^-} values of <30 s^{-1}), the *Cp* rubredoxin activation energies are plotted vs the free peptide value of 17 kcal/mol (black). With the exception of Val 38, all of these slowly exchanging sites are static solvent inaccessible.

For residues yielding activation energies in both *Cp* and *Pf* rubredoxins, the resultant differential conformational enthalpies of amide exchange are plotted against the protein sequence positions (Figure 5). At these sites, the red and blue symbols denote amides in the X-ray structures which are solvent accessible and inaccessible, respectively. Accurate activation energy measurements were not feasible for *Pf* rubredoxin amides having k_{OH^-} values of <30 s^{-1}. The activation energies of exchange for the corresponding residues of *Cp* rubredoxin are plotted relative to the free peptide value of 17 kcal/mol (denoted in black). In Figure 3B, the residues of *Cp* rubredoxin having conformational enthalpies at least 4 kcal/mol higher than in *Pf* rubredoxin are colored red. In orange are plotted the residues of *Cp* rubredoxin which have elevated activation energies of exchange that are more than 4 kcal/mole above the free peptide value; the corresponding exchange data of *Pf* rubredoxin are unavailable. Note that a cluster of 10 residues having elevated activation energy values in *Cp* rubredoxin forms a band around the metal site.

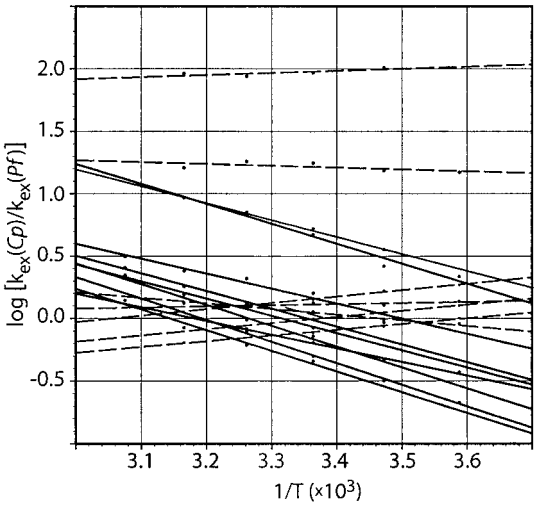

FIGURE 6: Arrhenius plot of the differential amide exchange kinetics for residues 14−32 of *Cp* and *Pf* rubredoxin. With one exception, the solid lines indicate the least-squares fit to data from residues for which the *Cp* rubredoxin log k_{OH^-} value is less than 3.0 at 23 °C, while dashed lines are used for more rapidly exchanging residues. Only Phe 30 exhibits a large negative slope combined with a log k_{OH^-} of >3.0 (for *Cp* rubredoxin).

More exceptional is the concentration of differential conformational enthalpies in the sequence region of residues 14−32. This protein segment is composed of a sequence of four contiguous turns, three characterized as 3_{10}-corners and residues 25−29 which form a glycine turn (*36*, *38*). As noted above, only in the hyperthermophile rubredoxin are the two ends of this segment linked by an ionic hydrogen bond between the carboxylate of Glu 15 and the main chain amide of Phe 30. The temperature dependence of the differential amide exchange rates for all of the non-proline residues of this protein segment is shown in Figure 6. For every residue, the data fit a linear dependence indicating no apparent temperature dependence of the underlying conformational enthalpies. The solid lines indicate the nine residues for which *Cp* rubredoxin has a 6.8 kcal/mol (rmsd of ±1.0 kcal/mol) higher conformational enthalpy. The seven residues denoted with dashed lines have much smaller differential conformational enthalpies [$Cp - Pf = -0.6$ kcal/mol (rmsd of ±1.3 kcal/mol)]. When compared to the exchange rate data of Figure 1, with the sole exception of Phe 30, all of the residues in the segment of amino acids 14−32 having elevated differential activation energies of exchange correspond exactly with the residues exhibiting the slowest exchange rates at 23 °C, clustered around 10 s^{-1} at pH 12.19.

In Table 1 are listed the exchange rate constants and the differential conformational enthalpies of exchange for the residues in the segment of amino acids 14−32. For residues 17−28 as well as for residue 14, the exchange rate constants are highly similar for both rubredoxins. Only those residues having log k_{OH^-} values near 2.8 (i.e., $k_{OH^-} = 630$ s^{-1}) have elevated activation energies in the mesophile protein. Deviations from this behavior occur only for positions adjacent to residues 15 and 30 near either end of this segment. Asp 16 of the *Pf* protein has a log k_{OH^-} value near 2.8, while the *Cp* Glu 16 shows a 100-fold increased exchange rate and a low activation energy. This difference in exchange rate presumably reflects the hydrogen bonding of the Glu 16 amide of *Cp* rubredoxin to the solvent accessible side chain carbonyl

Table 1: Amide Exchange Rate Constants (23 °C) and Differential Conformational Enthalpies (kilocalories per mole) of Amide Exchange for Residues 14−32 of *Cp* and *Pf* Rubredoxin[a]

residue	*Cp*	log k_{OH^-}	$\Delta\Delta H$	*Pf*	log k_{OH^-}
14	Asn	2.96	6.5	Asp	2.97
15	Pro			Glu	4.47
16	Glu	4.90	−0.8	Asp	2.93
17	Asp	3.00	5.5	Ala	2.80
18	Gly	2.82	6.3	Gly	2.89
19	Asp	2.75	7.6	Asp	2.89
20	Pro			Pro	
21	Asp	6.82	−2.1	Asp	6.93
22	Asn	3.80	2.1	Asn	3.75
23	Gly	6.09	−0.4	Gly	5.96
24	Val	2.80	5.0	Ile	2.99
25	Asn	6.86	−1.3	Ser	6.79
26	Pro			Pro	
27	Gly	2.94	7.5	Gly	3.28
28	Thr	2.67	7.9	Thr	2.97
29	Asp	5.26	0.7	Lys	4.13
30	Phe	3.83	6.0	Phe	3.02
31	Lys	5.49	−2.3	Glu	5.34
32	Asp	2.66	7.4	Glu	1.98

[a] With the exception of residue 16 for which the log k_{OH^-} values differ by 2 between the two rubredoxins, data for the same pH and temperature values were used to compare the two proteins at each residue position.

of Asn 14 rather than to the solvent inaccessible main chain carbonyl of Asp 14 as in the hyperthermophile protein. This switch in hydrogen bonding partners likely reflects the proline substitution at the intervening residue in the mesophile protein.

Although Phe 30 of *Pf* rubredoxin has a log k_{OH^-} values near 2.8, Phe 30 of *Cp* rubredoxin has a 6-fold higher rate constant and an elevated activation energy. In contrast to the hyperthermophile protein, in which the ionic hydrogen bond between the carboxylate of Glu 15 and the amide hydrogen of Phe 30 bridges between the ends of the segment of residues 14−32, the amide of Phe 30 in *Cp* rubredoxin is instead hydrogen bonded to the adjacent side chain carboxylate of Asp 29. Residue 32 exhibits an elevated activation energy in *Cp* rubredoxin. Furthermore, when compared to the remainder of this segment, residue 32 in both the *Cp* and *Pf* proteins shows a slightly lower log k_{OH^-} value, more similar to the values for the residues surrounding the metal site. This potentially indicates a transition toward the apparently more limited flexibility of that region. It should be noted that with the exceptions of residues 30 and 32, all of the slowly exchanging amides in the segment of amino acids 14−32 that have elevated activation energies in *Cp* rubredoxin exchange more rapidly in the hyperthermophile protein below room temperature (Figure 6).

Collective Conformational Opening in the Multiple-Turn Region of Rubredoxin. The slowly exchanging residues of the segment of residues 14−32 in *Cp* rubredoxin exhibit the combination of markedly similar exchange rate constants and similar differential enthalpies of conformational opening. This behavior is consistent with amide exchange occurring via a collective conformational transition. The residues showing more rapid exchange lack the increased activation energy, suggesting that the exchange behavior of these amides has not yet become entrained by the collective conformational transition, due to their having local fluctuations that are more exchange efficient. On the other hand, the hyperthermophile rubredoxin exhibits an equally striking constancy in the exchange rate constants for the more protected amides of the segment of residues 14−32 with k_{ex} values at 23 °C that are quite similar to those of *Cp* rubredoxin. For both proteins, residues preceding as well as those following this segment have significantly slower exchange rates, thus reinforcing the conclusion that the collective conformational transition of the segment of residues 14−32 cannot involve global unfolding. Rather, this segment is constrained at either end by the less flexible metal binding region. In both proteins, this segment opens to solvent accessibility with comparable exchange efficiencies but with a 6−7 kcal/mol difference in conformational enthalpy.

A physical mechanism which can potentially account for such a difference in conformational enthalpy between quite similar structures and sequences lies in the presumed solvent exposure of the buried Glu 15 carboxylate side chain of the hyperthermophile protein when its hydrogen bond to the Phe 30 amide is disrupted. The solvent ordering that underlies the hydration free energies of charged residues becomes markedly less favorable as the temperature is increased (*44*). Much of the discussion on this effect in the protein literature has focused on the resultant stabilization of ion pair interactions at elevated temperatures, although the same logic similarly applies to the case of an unpaired buried charge becoming exposed to bulk solvent. The amide of Phe 30 in *Cp* rubredoxin is also involved in an ionic hydrogen bond. However, its acceptor, the Asp 29 carboxylate, is highly solvent-exposed and hence would be expected to exhibit a smaller temperature dependence in its solvation free energy.

Calculation of the difference in the binding free energy for association of a protonated ethylamine and acetate salt bridge at 25 and 100 °C has yielded an enthalpy estimate of ~3 kcal/mol (*45*). In a similar calculation applied to the Sac7d protein from the hyperthermophilic *Sulfolobus acidocaldarius*, comparisons at 300 and 360 K for the sum of the solvation free energy and Coulombic energy at the seven glutamate residues yielded an average enthalpy of 6 kcal/mol, albeit with significant variation in the values for the individual residues (*46*). Such studies support the premise that the Glu 15−Phe 30 (+Trp 4 indole) interaction may largely account for a 6−7 kcal/mol difference in conformational enthalpy of amide exchange in the segment of amino acids 14−32 between the two rubredoxins.

Implications for Protein Thermostability. Below room temperature, the segment of residues 14−32 of *Pf* rubredoxin appears to be more flexible than its mesophile counterpart as detected by amide exchange processes with opening events that are rapid on the time scale of ~10 s^{-1}. More strikingly, more than one-third of the entire hyperthermophile protein appears to undergo a substantial conformational transition which has an equilibrium that is essentially temperature-independent over at least a 45 °C range, while for the corresponding segment of *Cp* rubredoxin, a significant temperature dependence is observed. Given the large difference in the time scale between the exchange reaction for the segment of residues 14−32 and the global unfolding reaction, this conformational transition cannot be very highly coupled to global stability. On the other hand, the implicit spatial scale of the motion of the segment of residues 14−32 suggests that its general energetic characteristics are

germane not only to native state fluctuations but also to the unfolding process. It should be noted that in the molecular dynamics simulations of *Pf* rubredoxin and a mesophile rubredoxin (*21*), separation of this multiple-turn sequence from the rest of the protein was predicted to be the initial step of thermal unfolding for both proteins.

Although discussions are commonly framed in terms of the evolution of protein thermostability, the genetic record appears to monitor primarily its loss. Ribosomal RNA sequence analysis indicates that the deepest known branches of the evolutionary tree are those of hyperthermophilic organisms (*47*). Furthermore, viable hyperthermophiles can be isolated from cold ocean waters (*48*, *49*). These observations support the hypothesis that the constituent proteins evolved under the double selective pressure of biological function near the boiling point of water combined with maintenance of structural integrity at lower temperatures to allow for migration between different marine thermal vent sites (*50*). Evolutionary expansion into more moderate growth temperature environments implies a more relaxed requirement for protein stability over a broad temperature range.

The data presented here indicate that the hyperthermophile rubredoxin has achieved comformational flexibility in the segment of residues 14−32 comparable to that of the mesophile homologue, but by a means having a much lower temperature dependence. Such a mechanism applied to the global unfolding transition would provide a "flattening" of the ΔG versus temperature profile, thus allowing for net stability over a wider temperature range without necessarily requiring an increase in the maximal thermodynamic stability (*51*).

ACKNOWLEDGMENT

We thank Marly Eidsness for providing the expression plasmids used in this work, Frederic Richards for providing the software for the solvent accessibility calculations, and James Prestegard for making available his manuscript prior to publication. We acknowledge the use of the Wadsworth Center NMR Facility and Protein Mass Spectrometry Facility.

SUPPORTING INFORMATION AVAILABLE

Table of exchange rate constants for all observed amides in *Cp* and *Pf* rubredoxins. This material is available free of charge via the Internet at http://pubs.acs.org.

REFERENCES

1. Jaenicke, R., Schurig, H., Beaucamp, N., and Ostendorp, R. (1996) *Adv. Protein Chem. 48*, 181−269.
2. Vieille, C., and Zeikus, G. J. (2001) *Microbiol. Mol. Biol. Rev. 65*, 1−43.
3. Sterner, R., and Liebl, W. (2001) *Crit. Rev. Biochem. Mol. Biol. 36*, 39−106.
4. Perutz, M. F., and Raidt, H. (1975) *Nature 255*, 256−258.
5. Yip, K. S. P., Stillman, T. J., Britton, K. L., Artymiuk, P. J., Baker, P. J., Sedelnikova, S. E., Engel, P. C., Pasquo, A., Chiaraluce, R., Consalvi, V., Scandurra, R., and Rice, D. W. (1995) *Structure 3*, 1147−1158.
6. Frankenberg, N., Welker, C., and Jaenicke, R. (1999) *FEBS Lett. 454*, 299−302.
7. Jaenicke, R., and Zavodszky, P. (1990) *FEBS Lett. 268*, 344−349.
8. Tang, K. E. S., and Dill, K. A. (1998) *J. Biomol. Struct. Dyn. 16*, 397−411.
9. Wrba, A., Schweiger, A., Schultes, V., Jaenicke, R., and Zavodszky, P. (1990) *Biochemistry 29*, 7584−7592.
10. Bonisch, H., Backmann, J., Kath, T., Naumann, D., and Schafer, G. (1996) *Arch. Biophys. Biochem. 333*, 75−84.
11. Zavodszky, P., Kardos, J., Svingor, A., and Petsko, G. A. (1998) *Proc. Natl. Acad. Sci. U.S.A. 95*, 7406−7411.
12. Jaenicke, R., and Bohm, G. (1998) *Curr. Opin. Struct. Biol. 8*, 738−748.
13. Varley, P. G., and Pain, R. H. (1991) *J. Mol. Biol. 220*, 531−538.
14. Gershenson, A., Schauerte, J. A., Giver, L., and Arnold, F. H. (2000) *Biochemistry 39*, 4658−4665.
15. Manco, G., Giosue, E., D'Auria, S., Herman, P., Carrea, G., and Rossi, M. (2000) *Arch. Biophys. Biochem. 373*, 182−192.
16. Fitter, J., and Heberle, J. (2000) *Biophys. J. 79*, 1629−1636.
17. Bai, Y., Sosnick, T. R., Mayne, L., and Englander, S. W. (1995) *Science 269*, 192−197.
18. Hollien, J., and Marqusee, S. (1999) *Proc. Natl. Acad. Sci. U.S.A. 96*, 13674−13678.
19. Chamberlain, A. K., Handel, T. M., and Marqusee, S. (1996) *Nat. Struct. Biol. 3*, 782−787.
20. Colombo, G., and Merz, K. M., Jr. (1999) *J. Am. Chem. Soc. 121*, 6895−6903.
21. Lazaridis, T., Lee, I., and Karplus, M. (1997) *Protein Sci. 6*, 2589−2605.
22. Hernández, G., Jenney, F. E., Jr., Adams, M. W. W., and LeMaster, D. M. (2000) *Proc. Natl. Acad. Sci. U.S.A. 97*, 3166−3170.
23. Hiller, R., Zhou, Z. H., Adams, M. W. W., and Englander, S. W. (1997) *Proc. Natl. Acad. Sci. U.S.A. 94*, 11329−11332.
24. Eidsness, M. K., O'Dell, S. E., Kurtz, D. M., Jr., Robson, R. L., and Scott, R. A. (1992) *Protein Eng. 5*, 367−371.
25. Eidsness, M. K., Richie, K. A., Burden, A. E., Kurtz, D. M., and Scott, R. A. (1997) *Biochemistry 36*, 10406−10413.
26. Lovenberg, W., and Sobel, B. E. (1965) *Proc. Natl. Acad. Sci. U.S.A. 54*, 193−199.
27. Pitzer, K. S. (1937) *J. Am. Chem. Soc. 59*, 2365−2371.
28. Barres, M., Redoute, J. P., Romanetti, R., Tachoire, H., and Zahra, C. (1973) *C. R. Acad. Sci., Ser. C 276*, 363−366.
29. Richie, K. A., Teng, Q., Elkin, C. J., and Kurtz, D. M., Jr. (1996) *Protein Sci. 5*, 883−894.
30. Hwang, T. L., Zijl, P. C. M. v., and Mori, S. (1998) *J. Biomol. NMR 11*, 221−226.
31. Mori, S., Abeygunawardana, C., Johnson, M. O., and Zijl, P. C. M. v. (1995) *J. Magn. Reson, Ser. B 108*, 94−98.
32. Hvidt, A., and Nielsen, S. O. (1966) *Adv. Protein Chem. 21*, 287−386.
33. Hwang, T. L., Mori, S., Shaka, A. J., and Zijl, P. C. M. v. (1997) *J. Am. Chem. Soc. 119*, 6203−6204.
34. Cavagnero, S., Debe, D. A., Zhou, Z. H., Adams, M. W. W., and Chan, S. I. (1998) *Biochemistry 37*, 3369−3376.
35. Lee, B., and Richards, F. M. (1971) *J. Mol. Biol. 55*, 379−400.
36. Watenpaugh, K. D., Sieker, L. C., and Jensen, L. H. (1980) *J. Mol. Biol. 138*, 615−633.
37. Bau, R., Rees, D. C., Kurtz, D. M., Scott, R. A., Huang, H. S., Adams, M. W. W., and Eidsness, M. K. (1998) *J. Biol. Inorg. Chem. 3*, 484−493.
38. Day, M. W., Hsu, B. T., Joshua-Tor, L., Park, J. B., Zhou, Z. H., Adams, M. W. W., and Rees, D. C. (1992) *Protein Sci. 1*, 1494−1507.
39. Strop, P., and Mayo, S. L. (1999) *J. Am. Chem. Soc. 121*, 2341−2345.
40. Zartler, E. R., Jenney, F. E., Jr., Terrell, M., Eidsness, M. K., Adams, M. W. W., and Prestegard, J. M. (2001) *Biochemistry 40*, 7279−7290.
41. Jung, D. H., Kang, N. S., and Jhon, M. S. (1997) *J. Phys. Chem. A 101*, 466−471.
42. Strop, P., and Mayo, S. L. (2000) *Biochemistry 39*, 1251−1255.
43. Bai, Y. W., Milne, J. S., Mayne, L., and Englander, S. W. (1993) *Proteins: Struct., Funct., Genet. 17*, 75−86.

44. Elcock, A. H., and McCammon, J. A. (1997) *J. Phys. Chem. B 101*, 9624−9634.
45. Elcock, A. H. (1998) *J. Mol. Biol. 284*, 489−502.
46. deBaker, P. I. W., Hunenberger, P. H., and McCammon, J. A. (1999) *J. Mol. Biol. 285*, 1811−1830.
47. Burggraf, S., Olsen, G. J., Stetter, K. O., and Woese, C. R. (1992) *Syst. Appl. Microbiol. 15*, 352−356.
48. Huber, R., Stoffers, P., Cheminee, J. L., Richnow, H. H., and Stetter, K. O. (1990) *Nature 345*, 179−182.
49. Stetter, K. O., Huber, R., Blochl, E., Kurr, M., Eden, R. D., Fielder, M., Cash, H., and Vance, I. (1993) *Nature 365*, 743−745.
50. Stetter, K. O. (1996) *FEMS Microbiol. Rev. 18*, 149−158.
51. Jaenicke, R. (1991) *Eur. J. Biochem. 202*, 715−728.
52. Connelly, G. P., Bai, Y., Jeng, M. F., and Englander, S. W. (1993) *Proteins 17*, 87−92.

BI0112560